ISSN: 3066-7194
Research Article
Novel Journal of Applied Sciences Research

Evaluation and Utilization of Iron Oxide Nanoparticles Impregnated onto Polyurethane for The Removal of Contaminants from River Wudil

Paul Ocheje Ameh

Department of Chemistry, Nigeria Police Academy, Wudil, P. M B. 3474, Kano State Nigeria

***Corresponding author:** Paul Ocheje Ameh, Department of Chemistry, Nigeria Police Academy, Wudil, P. M B. 3474, Kano State Nigeria.

Submitted: 16 September 2026 **Accepted:** 22 September 2026 **Published:** 28 September 2026

Citation: *Ameh, P. O. (2026). Evaluation and Utilization of Iron Oxide Nanoparticles Impregnated onto Polyurethane for The Removal of Contaminants from River Wudil. Nov Joun of Appl Sci Res, 3(5), 01-17.*

Abstract

The negative impact of water pollution is a major environmental concern for both nature and man. In recent years, there has been increased global concern about river water quality and quantity. This study is investigating the use of a new nanocomposite material (PUF - IONP) developed by loading iron oxide nanoparticles into a foam matrix of polyurethane (PU) to remove certain pollutants from River Wudil. The polyurethane foams used in the development of the composite was prepared by adding waste from the peel of plantain as a sustainable substitute for polyols. The formation of the PUF - IONP composite was confirmed by Brunauer, Emmett, and Teller (BET), X-ray diffraction (XRD), Fourier Transform Infrared Spectroscopy (FT-IR), Scanning Electron Microscopy (SEM), energy-dispersive X-ray spectroscopy (EDS), Thermogravimetric and differential thermo scanning calorimetry (TGA / DSC) analyses. The result obtained shows that the synthesized compound has a good ability to adsorb pollutants from the river water. PUF – IONP was found to significantly reduce turbidity, chemical oxygen demand, biochemical oxygen demand, Lead, Nickel, Cadmium by 98.89 %, 86.51 %, 59.44 %, 90.00 % , 83.33 % and 80.00 % respectively. Thermodynamic and kinetic study reveals that the adsorption of the pollutants was spontaneous, feasible, followed a second order kinetic model and is consistent with the mechanism of physical adsorption. It was also found that PU – IONP can be regenerated and reused in practical wastewater treatment due to its excellent adsorption performance and regeneration. The developed adsorbent which is a cheap, efficient, and environmentally benign adsorbent in removing pollutants from contaminated water, can contribute towards a novel approach in the waste water treatment process.

Keywords: Adsorption, Plaintain Peel Waste, Polyurethane, Remediation, River Wudil.

Introduction

Water contamination is a major problem, especially in developing countries like Nigeria, where people rely on surface water and groundwater for drinking and other household necessities [1]. There are so many biological, organic and inorganic pollutants that have been reported in literature as water contaminants [2, 3]. Some of them have serious side effects and toxicities with a few being lethal and carcinogenic. High levels of hazardous heavy metals are released into the environment by anthropogenic wastewater discharge, which affects the natural quality of soil and water and poses a direct or indirect risk to human health [4 – 6].

In addition to improving the availability of natural water sources, river water quality management and proper recovery can reduce the overall toxicity of soils and crops and provide a viable alternative to drinking water [7].

Extensive research work has been conducted to find and develop many separation and treatment techniques [8 – 11]. Methods such as precipitation and oxidation / reduction, and physical processes such as ion exchange and electro dialysis have been reported to be used in the treatment of various pollutants / contaminated waste water [12].

Nevertheless, most of these techniques have disadvantages, including incomplete removal of wastes, high consumption of reagents and energy, low selectivity, and generation of secondary wastes that are difficult to be eliminated [13].

Adsorption with activated carbon have been widely reported as the most commonly used material for the removal of heavy metals and dyes from contaminated water [14]. However, the high cost of commercial activated carbon and its importation to Nigeria have hampered its use in wastewater treatment [15].

Recently, polyurethane has been used to treat wastewater, thanks to its open porous structure, exceptional mechanical strength and high surface area, which makes it ideal for heavy metals, organic dyes and micro-plastics removal in industrial waste [16 - 19]. However, the synthesis of polyurethane foams is typically costly, because of the use of high-cost synthetic polyethylene glycols. One way to reduce the costs of their synthesis is to explore alternative synthetic methods which may include the use of renewable waste that will have adsorptive properties and the ability to decontaminate hydric bodies or treat effluents thus respecting environmental conservation.

One agro industrial waste that can be incorporated in the foams to serve as a substitute for polyols during the polymeric synthesis is plantain peel waste (PPW). This is due to the fact that PPW contains a number of hydroxyl groups that result from the presence of cellulose, hemicelluloses, pectin, and lignin [20]. Plantain peel is the main fruit residue in the plantain processing sector and represents 30 to 40 percent of total fruit waste [21]. In Northern Nigeria, the PPW generated are either fed to animals to a limited extent or disposed of as solid waste at great environmental cost. Finding the uses for these peels is therefore vital, if not essential, since they can exacerbate real ecological problems.

The purpose of the work was to synthesize and characterize a new nanocomposite material developed by loading iron oxide nanoparticles into a foam matrix of polyurethane (PU) to removal certain pollutants from the Wudil River. The inhabitants of Wudil, a city located in the northern part of Nigeria (Latitude 12.06532 oN and longitude 8.99484oE) use the river water for drinking, fishing, laundry, domestic use and irrigation [22]. The polyurethane foams used to develop the nanocomposite were prepared by adding the waste from plantain peels as a sustainable substitute for polyols. Characterization of the nanocomposite adsorbent was carried out using Brunauer, Emmett, and Teller (BET), X-ray diffraction (XRD), Fourier Transform Infrared Spectroscopy (FT-IR), Scanning Electron Microscopy (SEM), energy-dispersive X-ray spectroscopy (EDS), Thermogravimetric and differential thermo scanning calorimetry (TGA/DSC) analyses.

The simplicity and the upscalability of this process, use of readily available local raw materials, and use of inexpensive and non-toxic chemicals for this synthesis with the high-quality controllability make this novel approach a distinct process with a higher commercial viability

Materials and Methods

Collection of Raw Water Samples

The raw water samples were collected from the banks of the Wudil River in a clean plastic container. This was done by carefully dipping a wide mouth plastic container into the running water to collect the effluent. The pH and temperature of the water samples were determined directly using a pH meter (Jenway 3510) and mercury in glass thermometer respectively. The collected water samples were then filtered and acidified with 1.5 ml concentrated HNO_3 to preserve them and thereafter transported to the laboratory where they were stored in a refrigerator until analysis.

Determination of Physicochemical Parameters and Heavy Metals in The Water Sample

The pre-treated water samples were digested and determined for their physicochemical properties using standard methods as described by the American Public Health Association [23]. The total alkalinity, hardness and chloride were estimated using the method as described by American Public Health Association. The nitrate and phosphate levels were measured using a Wagtech Photometer (model CP 1000). A portable mercury glass thermometer (model U7, Horiba Ltd) was used to measure the temperature at the source. The Total dissolved solids (TDS), Dissolved oxygen and conductivity were measured with TDS meter (Hanna instrument), Wagtech turbidimeter (model CP1000) and Conductivity meter (Jenway model) respectively. The atomic absorption spectrophotometer (Analyst 100 Perkin Elmer) was used to determine the number of heavy metals in the effluent following the methods described in the manufacturers' instruction manual.

Collection and Preparation of Plantain Peel Waste (Ppw) / Iron Oxide Nanoparticles (Ionps)

Musa paradisiaca (plantain) was obtained from Sabon gari market in Kano metropolis of Northern Nigeria. The peel was removed, washed in clean water and cut into small pieces. The chopped peel was air-dried for two weeks, macerated into a fine powder by a high-speed multipurpose blender and then stored in a refrigerator for further investigation. The iron oxide nanoparticles (IONPs) used in this study was the one prepared and reported by Ameh [24].

Synthesis and Characterization of Polyurethane Iron oxide Nanocomposite (PUF - IONP)

6.0 g of PPW was transferred into a beaker and molten at 50 °C. After cooling, 0.6 mL of polymethylhydrosiloxane (PMHS) and 0.10 mL of glycerol were added to it. In another separate beaker, 3.0 g of methylene diisocyanate (MDI) was molten at 50°C. After it was cooled, 0.30 mL of tin octoate catalyst was added. The content of the two beakers were subsequently mixed together. Different weight percentages (1, 5 and 10 %) of IONP were then added manually to the resulting mixture and agitated vigorously until the foam grew. The resulting PUF – IONP formed was left to at rest for 24 hours at room temperature and stored until further use. The same procedure was used in the synthesis of the polyurethane (PU); but in this case, no IONP was added.

Adsorbent Characterization

The specific surface area of IONP, PU and PU - IONP was examined by the Brunauer, Emmett, and Teller (BET) multipoint method using Nova 2000 Surface Area Analyzer (Quantachrome Instrument Version 11.03). X-ray diffraction analysis was carried out to determine their crystallinity using an X-ray diffractometer (Panalytical X'Pert Pro X-ray diffractometer, Netherlands) with a Cu target (1.5406 Å) in the 2θ range of 3.50º to 89.99º and at a scan rate of 0.01°/min. The FTIR spectra were recorded using a Fourier-transform infrared (FTIR- Agilent Cary 630 FTIR)

spectrometer in the range of 4000–400 cm^{-1} with a spectral resolution of 4 cm−1at room temperature to get insight into interactions between the polyurethane and iron oxide nano particle. The morphologies of the adsorbent were assessed at an acceleration voltage of 20 kV by scanning electron microscopy (SEM) (SEM 800-07334 instrument, Phenomworld, Nertherlands) coupled with energy-dispersive X-ray spectroscopy (EDS) for elemental composition analysis. Atomic adsorption spectrophotometer (AA-480 FS, Agilent Technologies, US) was used for determination of the heavy metals in the raw and treated water samples. Thermogravimetric and differential thermo scanning calorimetry analyses (TGA/DSC) were carried out to determine the thermal behavior of the nanocomposite using a Mettler-Toledo instru¬ment (Greifensee, Switzerland) in the range of 20–1000 ◦C at a heating rate of 10◦C / min under a nitrogen atmosphere.

Batch Adsorption Studies

The Batch adsorption studies were performed by making the river water passed through polyurethane – iron oxide nanoparticle pellet (adsorbent) placed in a plastic syringe and thereafter shaked with an Innova 4000 incubator shaker operating at 180 revolution per minute (rpm) agitation speed.

To optimize the experimental conditions for the removal of some metal ions (i.e. Cr^{2+} , Cd^{2+} and Pb^{2+}) from the effluent, various parameters such as pH in the range of 2 to 12, contact time from 10 minutes to 100 minutes, the dose of PUF - IONP foam (0.5–3.0 g) and different concentrations of heavy metal solutions (i.e., 100 ppb, 200 ppb, 400 ppb, and 600 ppb). The residual concentration of the metal ions in the solution was determined using atomic absorption spectrometer.

The removal efficiency (%) of heavy metal ions and adsorption capacity (q_e) of the prepared PUF – IONP were thereafter estimated using equation 1 and 2 respectively

$$\text{Removal efficiency (\%)} = \frac{C_i - C_e}{C_i} \; x \quad 100 \tag{1}$$

$$q_e \left(\frac{mg}{g}\right) = \frac{C_i - C_e}{M} \; x \; V \tag{2}$$

where the initial and equilibrium metal ion concentrations in the solution (mg L^{-1}) are C_i and C_e. M is the mass in grams of the adsorbent used and V is the volume in Litres of the effluent solution.

Regeneration and Reusability Studies

Regeneration and reusability studies were carried out as described by Song et al 2020. In the desorption study, Cr(VI), Pb(II) and Cd(II) ions loaded PUF - IONP were initially washed three times with distilled water to eliminate any loosely attached metal ions from their surface. The desorption process involved mixing 0.05 g of studied metal ions – loaded PUF - IONP with 10ml of 0.1 M HCl for 1 hour on a shaker at an agitation speed of 180 rpm at room temperature. Desorption efficiency was evaluated using equation 3.

$$\text{Desorption efficiency (\%)} = \frac{Concentration\ of\ released\ metal\ ions}{initial\ concentration\ of\ adsorbed\ metal\ ion} \; x \quad 100 \tag{3}$$

The regenerated PUF - IONP were tested for the reusability process by following the adsorption – desorption process for several cycles for each of the studied metal removal.

Results and Discussion

Characterization of Adsorbent

FTIR Study

Fourier transform infrared spectroscopy was applied to determine / monitor the changes of the chemical compositions of the synthesized polyurethane based adsorbent before and after the addition of IONP. Figure 1 show the FTIR spectra obtained for IONP, PU and different composition of PU –IONP composite. The frequencies and functional group assignments of peaks deduced from the adsorption spectra are presented in Table 1. In the IONP spectra, strong absorption peaks at 572 cm^{-1} and 3423 cm-1 attributed to Fe–O bond stretch and O–H stretch respectively in the iron oxide nanoparticle were observed. Other notable absorption bands observed included = C –H aliphatic stretch at 2853 cm^{-1}, free - C = O stretch at 1695 cm^{-1} , C – H in plane bend at 1424 cm^{-1} and C– O stretching at 1023 cm^{-1} which is consistent with that reported by Mishra et al (2014) to confirm the formation of iron oxide nanoparticles. The FTIR spectrum of polyurethane (PU) indicated the presence absorption bands ascribed to –C– O – C stretching, –CH_2 deformation, - N – H bend, - C = C stretch, - C = O stretch, –CH_2 stretch, asymmetric C – H stretch and - N – H bond stretch . The absence of the characteristic peaks of IONP (572 cm^{-1}) from the PU – IONP spectra may indicate its complete incorporation our synthesized polymer composite, without a significant contribution to the surfaces, due to the covering of the IONP with the polyurethane

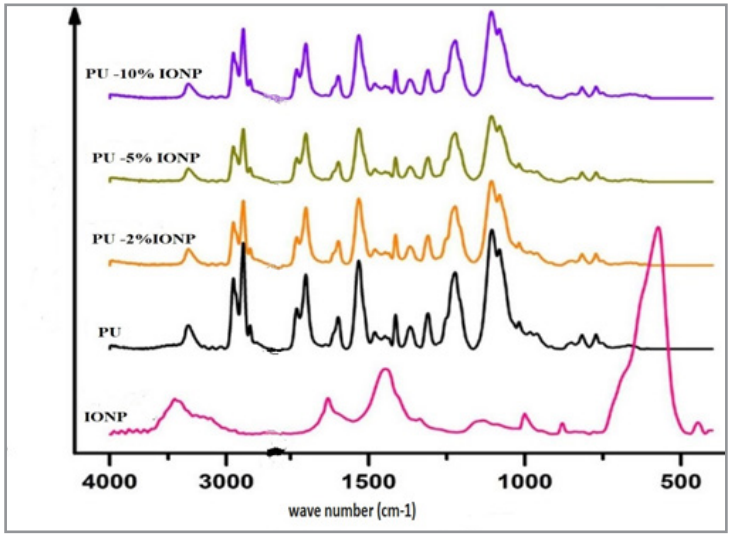

Figure 1: FTIR Spectra of IONP, PU and PU –IONP Composite

Table 1: Frequencies and Functional Group Assignments of Peaks Deduced from IR Adsorption Spectra Of IONP, Pu and Pu –IONP Composite

Frequencies (cm^{-1})					FUNCTIONAL GROUP ASSIGNMENT
IONP	PU	PU – 2% IONP	PU – 5% IONP	PU – 10% IONP	
572					Fe – O stretch
872					=CH out of plane bending
1023					–C– O stretching
	1031	1032	1030	1031	–C– O – C stretching
	1107	1107	1106	1107	–C– O – C stretching
	1310	1311	1311	1311	–CH2 deformation
	1412	1412	1412	1413	–CH2 deformation
1424					- C – H in plane bend
	1532				- N – H bend
	1597				- C = C stretch
1695	1700	1702	1703	1702	free - C = O stretch
	1731	1732	1731	1732	bonded - C = O stretch
	2854	2856	2855	2855	symmetric –CH2 stretch
	2940	2941	2942	2941	asymmetric C – H stretch
2853					= C –H aliphatic stretch
	3326	3326	3326	3327	- N – H stretch
3422					O – H stretch

Scanning Electron Microscopy (SEM) / Energy – dispersive X-ray spectroscopy (EDS) Analysis

The surface morphology of the PU, IONP and PU – IONP was confirmed by SEM study. Figure 2 shows the SEM images that can give an insight about the aspect of the surfaces of the synthesized PU, IONP and PU – IONP that were implemented as adsorbents for the removal of contaminants from River Wudil. It can be observed from the images presented that PU (Figure 2(a)) and IONP (Figure 2(b)) both has irregular and uneven pores. The pores identified in the PU loaded IONP (Figure 2C & D) became more evenly distributed in the matrix. The IONPs according to Dinali et al [25] is acting as a nucleating agent, generating a uniform distribution of pores at the surface of the composite. A significantly increased surface areas and material pore volumes could also be observed in the PU – IONP micrograph. The improved porous structure of PU – IONP is a pointer that it will be a good adsorbent for the treatment of waste water [26].

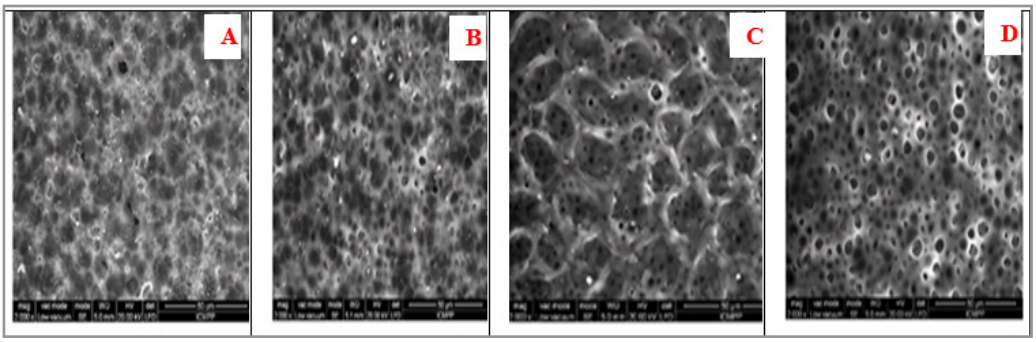

Figure 2: SEM images of (a) PU (B) IONP (C) PU – 2% IONP (D) PU – 10% IONP

The EDS component of the SEM 800-07334 instrument was exploited to reveal the elemental composition of the synthesized nanocomposite. The result obtained showed that PU – IONP contain a significant percentage of carbon (83.54%) when compared to other elements such as oxygen (13.30 %), chlorine (1.06 %), iron (0.95%), silicon (0.58 %) and tin (0.57%). The high carbon content observed is attributed to the carbon-containing compounds in polyurethane.

The observed signals of oxygen and iron must have originated from iron oxide nanoparticles (IONPs). The traces of tin and chlorine detected could have come from tin chloride pentahedrate. As no other elements other than those expected were present, it can be concluded that the synthesized PU – IONP does not contain any impurities.

X-ray Diffraction (XRD) Study

The XRD patterns obtained for polyurethane foam (PU), synthesized iron oxide nanoparticles (IONP) and various percentages of polyurethane foam – iron oxide nanocomposite (PU – IONP) are shown in Figure 3. The XRD pattern of PU revealed the broad peak at approximately 2θ equal to 20.6◦ which according to Athir et al (2020) is indicative of a typical low - crystalline structure or material. The diffractogram of the IONP exhibited

diffraction peaks at 2θ equal values of 24.13°, 33.11°, 35.27°, 40.71°, 49.37°, 53.72°, 57.83°, 62.41°, and 63.85°, corresponding to (011), (103), (111), (112), (023), (117), (019), (213), and (301) planes, which are consistent with the standard pattern of Fe_3O_4 [27]. The PUF – IONP is a polyurethane foam coated with Fe_3O_4. A closer examination of the XRD patterns obtained for PUF – IONP shows that there are additional peaks in PUF – IONP which are not present in those obtained for PU. This may be due to the addition of IONPs as additional peaks observed in PUF-IONP are also present in IONPs. This implies that PUF – IONP is actually a polyurethane foam that has been coated with Fe_3O_4. Another notable from the XRD results obtained is that intensity of the PUF – IONP increased as the amount of iron oxide nano-particles increased in composite.

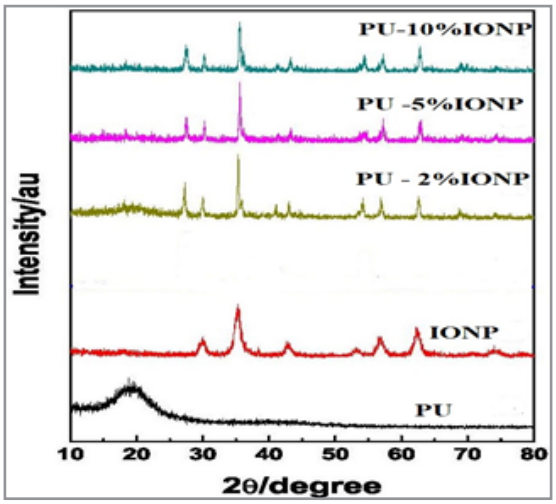

Figure 3: X-ray Diffraction Curves of (a)PU (b) IONP (c) PU – IONP

Bruneur-Emmette-Teller (BET) Analysis

The BET analysis was performed to determine the surface area of the nanocomposite which was synthesized to remove the contaminants from the river water. Table 2 shows the results obtained from the BET analysis of PU, IONP and PU – 10 % IONP composite. A closer look at the table shows that PU – 10 % IONP with a value of 706.372 m²/g has the highest surface area, followed by PU with 410.341 m²/g and then IONP with a surface area of 347.360 m²/g. PU – 10 % IONP was also found to have the highest pore size (5.413 nm) followed by PU (4.350 nm) and then IONP (4.107 nm). The presence of PU in the composite, which serves as the substrate to which the IONP particles attach to, gives PU a larger surface area and pore volume than IONP and is thought to contribute more to the active adsorption of contaminants by the composite (PU-IONP) than IONP. It should also be noted that the surface area of the PU-IONP composite obtained in this study was within the ASTM recommended range of 600 - 1200 m² per g for highly adsorbent materials.

Table 2: BET Results for of PU, IONP and PU – IONP composite

Sample	BET surface Area (m²/g)	Pore Volume(cc/g)	Pore Size (nm)
PU	347.360	12.561	4.350
IONP	410.341	14.311	4.107
PU – 2 % IONP composite	683.145	20.011	4.945
PU – 5 % IONP composite	700.252	21.825	5.177
PU – 10 % IONP composite	706.372	23.570	5.413

Thermo -Gravimetric Analysis

Thermo-gravimetric analysis (TGA) is often used to rank polymers in order of thermal stability by comparing the loss of mass with the temperature. To test the formation of the PU and PU-IONP composite synthesized in this study and to investigate its thermal stability, the thermal behaviour of both PU and PU-IONP composite was measured by means of TGA and differential scanning calorimetry (DSC).

Figures 4 and 5 gives the TGA and DSC images obtained for PU and PU loaded with different concentrations of IONP. A closer examination of the graphs submitted shows the degradation of PU and PU–IONP proceeded via two major stages which can be attributed to the thermodynamically incompatibility of the soft and hard domains in polyurethane. The first step of weight loss which occurs at a temperature maximum of 317.6 ◦C, 326.9 ◦C and 328.5 ◦C (see Figure 4) for PU, PU – 5 % IONP and PU – 10 % IONP respectively is attributed to the depolycondensation reaction of polyurethane to produce precursors such as polyols and isocyanates (degradation of the soft domain in polyurethane). The second step occurring at 414.2 ◦C, 420.4 ◦C and 423.6 ◦C for PU, PU – 5 % IONP and PU – 10 % IONP respectively can be associated with the decomposition of the substituted urea in polyurethane (degradation of the hard domain in polyurethane). The observed slight shift in the thermal degradation of PU and PU coated IONP could be due to the incorporation of IONPs into the PU and a pointer that the addition of iron oxide nano particle into the PU matrix enhanced the thermal stability of the PU in the nanocomposite.

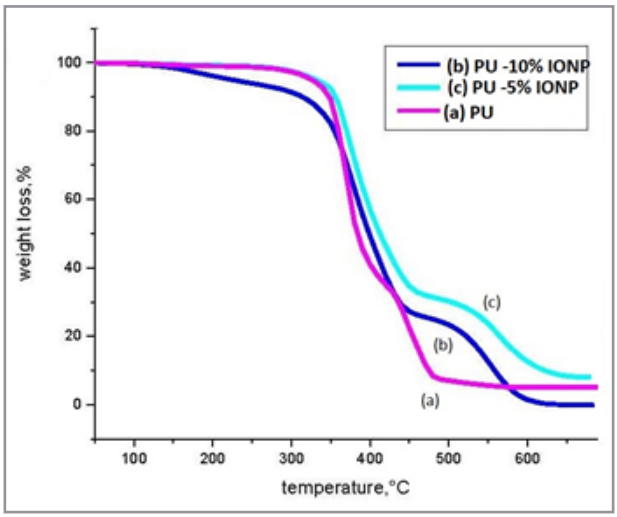

Figures 4: TGA thermographs of (a) PU (b) PU – 5 % IONP (c) PU – 10 % IONP

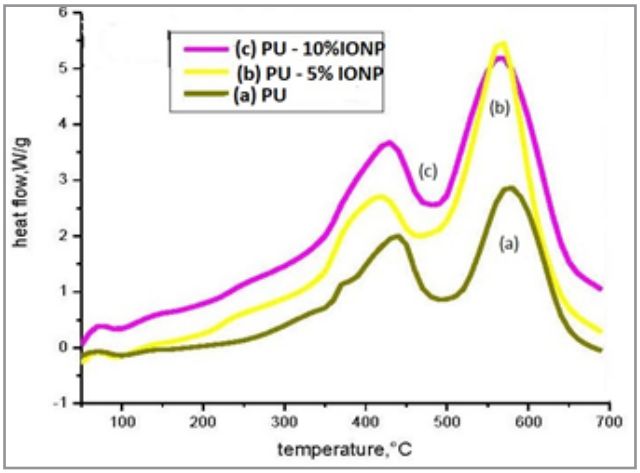

Figures 5: DSC Scans of (a) PU (b) PU – 5 % IONP (c) PU – 10 % IONP

Characterization of Raw Water Collected from River Wudil before Treatment

The results for physicochemical characterization of the water collected from Wudil River are as presented in Table 3. A closer examination of the table shows that the average temperature of the water was 35.18°C, a value that is above the WHO recommended limit of 30.00°C. According to Jamila and Sule [28], temperature plays an important role in regulating the chemical reactions in water and the metabolic processes of fish. The increase in temperature normally leads to algal growth that stifles aquatic organisms, while the decrease in temperature allows most substances to become insoluble in the water [29]. The values of pH, electrical conductivity and turbidity from the study were found to be 6.47 and 1788.70 μScm^{-1} and 6.08 NTU respectively. These values are also outside the safe levels of drinking water as set by National Environmental Standards and Regulations Enforcement Agency [30] and World Health Organization [31]. The lower pH values obtained may increase water corrosion and metal bioavailability. The high conductivity and turbidity values could be linked to ions containing wastes often dumped into the Wudil River. The values of Dissolves oxygen (DO), Biochemical oxygen demand (BOD) and Chemical Oxygen Demand (COD) were found to be 4.11, 2.17, 8.89 mg/l respectively. The low values of DO and higher values of COD when compared to the World Health Organization permissible limits indicates that the river water is highly polluted [31]. It is been reported that water bodies with BOD levels between 1.0 and 2.0 mg/l are usually considered clean, those with BOD values of 2 – 3 mg/l are fairly clean, 5.0 mg/l doubtful and 10.0 mg/l definitely bad and polluted [32]. Based on the BOD values obtained in the study, we can say that the purity of the water is doubtful. The Total dissolved solids (TDS) value which provides information on the aesthetic value, turbidity status and density of the studied River water was found to be 1205.05 mg/L. This observed high TDS is a pointer that the river water contains high number of pollutants, dissolved solids, ions and inorganic salts which can cause a reduction in the development and survival of salmond eggs and larva and clogging on fish gills. The alkalinity values obtained in the entire study area were low as compared to WHO permissible limit of 500 mg/l set for alkalinity in water. The acidity values which is a measure of the presence of free CO_2 and dissolution of carbonate rocks was found to be 97.33. Higher acidity value of water according to Ibrahim, and Sa'id [33] does not support the survival of aquatic life. The high sulphate level observed in the study which can causes diarrhea must have come from mostly run off of human waste. The NO_3^- values obtained in this study when compared with the WHO permissible limits of 50 mg/l for nitrate in water showed that the water from Wudil river are not safe for drinking. The source of high nitrate level in the river could be traced to the use of nitrous based fertilizer in farms for plant growth in the area. The observed PO_4^{2-} value of 349.25 mg/l which is higher than WHO and NESREA limits

can seriously contribute towards the eutrophication of the river under study. The mean level of Cl^- was found to be 733 mg/l whereas the WHO permissible limit of Cl- in water is 200 mg/l. The negative effect of too much chloride in surface water is that it breaks up organic matter thereby restrain algae growth, cause infertility in fish eggs, fasten corrosion of metal and also affect plant growth. The values of potassium (9.22 mg/l) and calcium (33.15 mg/l) obtained were within the WHO permissible limit.

The results from the heavy metal analysis indicated that the river water is said to be polluted with Cd, Pb Ni and Fe when their values are compared to standard limits set by WHO and NESREA for drinking water. The high content of some of these heavy metals in water observed may be due to run – off / flooding through mechanic workshops, construction sites close to water, frequent washing of car engines at the car wash close to the river bank, dumping of already used lead batteries and other metal containing wastes into the river. Generally high concentration of heavy metals in River water usually accounts for most of the cases of pediatrics metal poisoning and targets bones, brain, kidney and thyroid glands in humans. It is interesting to note that the heavy metals concentrations analyzed in the river water under study were at par with values reported for similar metals in water of River Jakara, Kusalla dam and River Getsi all in Kano State Nigeria. However, the values for similar heavy metals obtained in the study area were lower than those of River Gwagwarwa and River Kubani Dam [34]. It can be said that as far as heavy metals bioaccumulation in drinking water is concern, water from River Wudil must be treated before consumption.

Table 3: Physicochemical Characteristics of Surface Water from Wudil River

S/N	PARAMETERS	Raw River wudil Water	Treated River Wudil Water	Percentage removal (%)	WHO standard
1	Temp (°C)	35.18	29.90	-	30.00
2	pH	6.47	6.8	-	6.5 – 8.5
3	Electrical conductivity (µScm-1)	1788.70	272.51	84.76	1400
4	Acidity (mg/l)	97.33	32.22	66.90	50
5	Alkalinity(mg/l)	133.00	56	57.89	500
6	TDS (mg/l)	1205.05	216	82.08	1200
7	Turbidity (NTU)	18.08	0.20	98.89	5
8	DO (mg/l)	9.26	4.1	55.72	5
9	BOD (mg/l)	2.17	1.02	59.44	28-30
10	COD (mg/l)	48.92	6.6	86.51	8
11	$SO_4^{2-}\left(\frac{mg}{l}\right)$	536.28	78.5	85.36	500
12	$PO_4^{2-}\left(\frac{mg}{l}\right)$	349.25	2.98	99.15	250
13	$Cl^-\left(\frac{mg}{l}\right)$	733	50.8	93.07	250
14	$NO_3^-\left(\frac{mg}{l}\right)$	57.27	12.5	78.17	50
15	K (mg/l)	9.22	7.56	18.00	20
16	Ca (mg/l)	33.15	18.55	44.04	50
17	Na (mg/l)	3.51	2.50	28.77	2.5
18	Mg (mg/l)	5.22	0.17	96.74	0.20
19	Fe (mg/l)	0.63	0.21	66.67	0.30
20	Pb (mg/l)	0.10	0.01	90.00	0.01
21	Cu (mg/l)	0.04	0.02	50.00	1.00
22	Co (mg/l)	0.02	0.01	50.00	0.02
23	Cr (mg/l)	0.03	0.02	33.33	0.05
24	Cd (mg/l)	0.06	0.01	83.33	0.00
25	Ni (mg/l)	0.05	0.01	80.00	0.02
26	Mn	0.04	0.02	50.00	0.2
27	Zn	2.11	0.89	57.82	3.00

Performance Analysis

The results from the physicochemical analysis of the water collected from River Wudil indicates that the water contains high concentrations of pollutants which might have cause increase in biological oxygen demand, chemical oxygen demand, total dissolved solids, total suspended solids and makes it unfit for drinking and irrigation. The performance of the synthesized PU – IONP was accessed by passing the river water through a layer of it with the impacts examined. The percentage contaminant removal achieved after treating the river water collected with

PU – IONP is as presented in Table 3. It can be seen from the results presented those enhanced values of heavy metals, TDS, turbidity, COD, DO, phosphate and conductivity was obtained for the river water after treatment with PU – IONP thus confirming the high adsorption ability of the prepared composite. The synthesized composite could eliminate 98.89 % turbidity, 90.00 % of Pb, 83.33 % of Ni and 80. 00 % of Cd, 55.72 % of DO, 59.44% of BOD, 86.51% of COD. The reason for the ability of PU – IONP to treat pollutants in wastewater may be as result of the presence of multiple functional groups, polyphenols high surface area and pore volume as revealed during its characterization that can absorb mineral ions and dissolved organic matter in water.

Batch Equilibrium Studies

Batch adsorption studies were carried out in order to understand the mechanism of adsorption through isotherm, thermodynamics, equilibrium and kinetic studies. The contributions of the period of contact, initial metal ion concentration, pH and the weight of PU – IONP for the removal of Cd (II), Cr (VI) and Pb (II) ions which were discovered exceeded the maximum permissible limits in the river water were investigated by varying these factors over reasonable range The kinetic study was done using the pseudo-first order, pseudo-second order and intra-particle diffusion models respectively while the equilibrium study was performed using the Langmuir, Freundlich and Dubinin–Radushkevich isotherm

Effect of pH Variation

Table 4 shows the variation in the percentage of Cr (VI), Pb (II) and Cd (II) ions removed from the river effluent by different composition of PU – IONP with solution pH. It can be deduced from the result obtained that PU – IONP possesses high removal of the metal ions at lower pH. Removal of Cd (II), Cr (VI) and Pb (II) by PU – IONP is observed to be at optimum pH of 5, 4 and 5 respectively. The increase in studied metal ions removal as the pH increases from 1 to 5 can be explained on the basis of a decrease in competition between proton and the metal cation for the surface sites and as well as by the decrease in positive surface charge which results in a lower coulombic repulsion of the sorbing metal cations [35]. The increased adsorption of the adsorbent at low pH may also be attributed to the surface of PUF – IONP containing some phenolic or carboxylic functional groups as revealed by the FTIR. The possible precipitation of the studied metal ions as hydroxide salts at higher pH may have predominantly led to the decrease in uptake or removal of the ions from pH 6 -12. The 10 % loaded IONP – PU adsorbent yielded a higher removal capacity when compared to the 2 % and 5 % loaded IONP – PU.

Table 4: Percentage of Cr (VI), Pb (II) and Cd (II) ions removed from the effluent by different composition of the adsorbent at various pH

pH	PU – 2 % IONP composite			PU – 5 % IONP composite			PU – 10 % IONP composite		
	Cr (VI)	Cd (II)	Pb (II)	Cr (VI)	Cd (II)	Pb (II)	Cr (VI)	Cd (II)	Pb (II)
2	97.8718	95.1456	97.2424	98.9802	97.8343	98.8817	99.9100	99.4446	99.7211
3	98.2016	96.8812	98.9912	99.7116	98.3267	99.0592	99.9991	99.9528	99.9852
4	98.9224	97.4445	99.1022	99.9991	99.7420	99.8490	100.000	99.9992	99.9999
5	98.4084	97.6764	98.2448	98.8942	99.7771	99.5149	99.9246	99.9993	99.9145
6	98.0017	97.6279	97.6937	98.5213	98.5645	98.4067	98.9607	99.8902	98.9256
7	97.9809	97.6048	97.6138	98.3269	98.4554	98.3072	98.8051	98.2041	98.3818
8	90.5004	89.5821	91.1515	93.1006	91.4446	92.7204	95.6933	93.1455	94.1061
9	89.5621	88.7145	89.2506	92.4301	90.9528	91.3527	94.5741	92.0411	94.0172
10	89.3515	87.9901	88.5438	91.7848	89.9052	90.9228	93.9924	91.0655	92.6150
11	88.8824	86.5415	87.0698	90.1146	88.9911	89.5993	92.5576	91.0588	91.7137
12	87.3308	86.6228	86.3505	89.6074	87.6902	89.0325	92.0510	90.8477	91.1817

Effect of Metal Ions Concentration Variation

To investigate the effect of using different concentrations of heavy metal solutions (i.e., 100 ppb, 200 ppb, 400 ppb, and 600 ppb) on the percentage removal efficiency of Cd (II), Cr (VI) and Pb (II) from the synthetic multi elemental wastewater by the adsorbent, one gram of IONP – PU was kept in contact with the metal ions solutions for 30 minutes. The variation of amount of heavy metal ion adsorbed by PU – 10 % IONP with concentration of the studied metal ions in solution is presented in Figure 6. The figure shows that the removal capacity of PUF – IONP increases at the beginning as the concentration of the metal ions in solution is being increased. However, further increase in the ion concentration in solution led to a significant decrease in its adsorption. These observed phenomena can be attributed to the increase in the concentration of the adsorbate as against a fixed number of available active sites on the adsorbent. This result is in good agreement with literature [36].

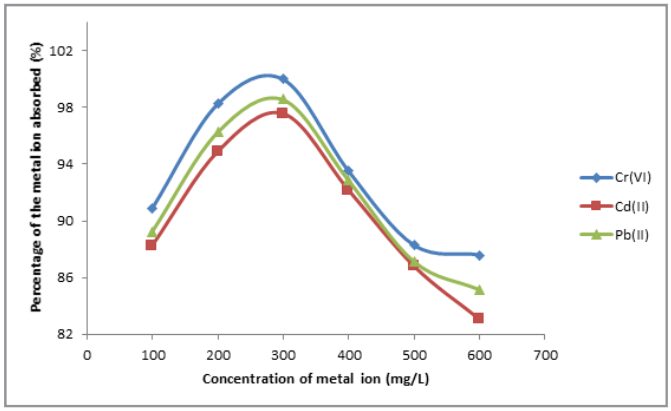

Figure 6: Variation of Amount of Heavy Metal Ion Adsorbed by Pu – 10% IONP with Concentration of The Metal Ions in Solu-

Effect of PUF - IONP Weight on Adsorption

To study the effect of using different sample weights on the removal capacity of Cd (II), Cr (VI) and Pb (II), six different weight (0.5, 1.0, 1.5, 2.0, 2.5 and 3.0 g) of 10 % IONP – PU composite were prepared and soaked in a solution containing 100 mg/L each of Cd (II), Cr (VI) and Pb (II) for 30 minutes. Figure 7 presents plots obtained for the variation of the concentration of heavy metal ions adsorbed with weight of PU – IONP. It can be observed that the percentage removal of the various studied metal ions from aqueous solution increased with increase in the weight of PU – IONP. For instant, the removed amount of Pb (II) was found to increase from 20 mg/L to 70 mg/L, when the weight of PU – IONP increased from 0.5 g to 3 g; respectively. The metal increment in adsorption capacity with increase in adsorbent dosage of the studied metal ions was expected. This is because increase in the weight of PU - IONP implies increase in the adsorbent particles and hence more surface areas were available for metals attachment. This trend is similar to the ones reported in literature [37].

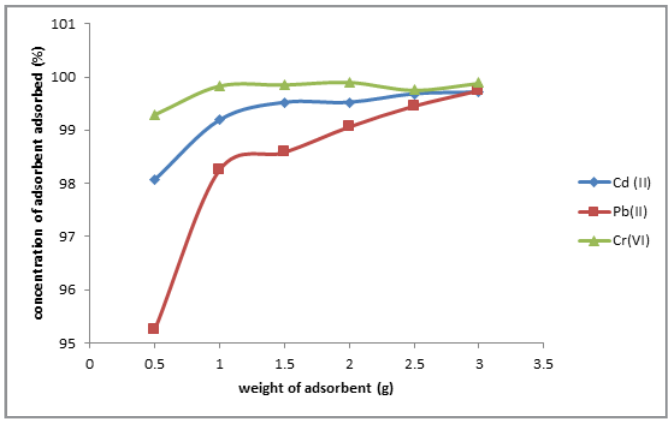

Figure 7: Variation of the concentration of adsorbed heavy metal ions adsorbed with weight of PU – 10 % IONP

Effect of Contact Time

It has been found that the period of contact of adsorbates and adsorbents is of great importance in adsorption study because it depends on the nature of the system used. The effect of contact time on the removal capacity of Cd (II), Cr (VI) and Pb (II) were studied in the range of 20 minutes to 100 minutes exposure time using 1-gram PU – IONP composite. Figure 8 show plots for the variation of the amount of the studied metals ions adsorbed unto the composite with time. From the figure presented, it can be seen that the amount of Cd (II), Cr (VI) and Pb (II) ions adsorbed were found to increase progressively with time. The rate of adsorption was however was rapid in the first 20 minutes after which the rate slowed down as the equilibrium state was approached. The order of adsorption of the metal ions by PU – IONP followed this order: Cr (VI) > Pb (II) > Cd (II).

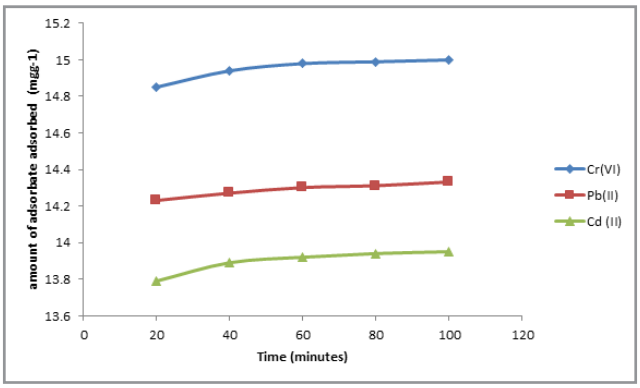

Figure 8: Variation of the amount of metal ion adsorbed per unit mass of PU – IONP with time

Sorption Kinetics Study

In order to examine the kinetic mechanism which controls the adsorption process, kinetic models like pseudo - first – order, pseudo-second-order and intra-particle diffusion were tested to interpret the experimental data. The linear forms of the listed models are represented by equation 4, 5, and 6 while the respective plots obtained are shown in Figures 9 – 11 respectively [38 – 40].

$$\log(q_e - q_t) = \log(q_e) - \left(\frac{k_1}{2.303}\right)t \quad (4)$$

$$\frac{t}{q_e} = \left(\frac{1}{k_2 q_e^2}\right) + \left(\frac{1}{q_e}\right)t \quad (5)$$

$$q_t = k_{in}\sqrt{t} + \beta \quad (6)$$

Where k_in (in mg/g $min^{½}$) is the intraparticle diffusion rate constant, k_1 (in min^{-1}) is the pseudo-first order rate constant, k_2 (in gmg-1min^{-1}) is the pseudo-second order rate constant, β (in mg/g) is related to the thickness of the boundary layer, q_e and q_t are respectively the amount of heavy metal ions in mg/g adsorbed at equilibrium and at time, t.

The evaluation of the best fit kinetic model was made based on the regression coefficient (R^2) values obtained from the plots. Table 5 summarizes the calculated values of R^2, k_{in}, k_1 , k_2, β and q_e calculated from the slope and intercept of the kinetic model plots (Figure 9 – 10). As seen in the results presented, the calculated values of R^2 for the pseudo – second-order are higher than those obtained for the other two models implying that the adsorption kinetics of the synthesized adsorbent is better represented by the second order kinetic model. Furthermore, the q_e values calculated from the second order kinetic model were found to reasonably agree well with those obtained experimentally. This further support that the adsorption of Cd (II), Cr (VI) and Pb (II) onto PU - IONP follow the pseudo second – order model.

The pseudo - second order rate constant (k_2) of the adsorbed metal ions by PU – IONP as reported in Table 5 followed this order: Cr (VI) > Cd (II) > Pb (II). This implies that the uptake of Cr (VI) onto PU - IONP from the aqueous solution was more rapid and favourable.

The intraparticle diffusion linear plots (Figure 11) obtained for Cd (II), Cr (VI) and Pb (II) did not pass through the origin. This means that there were differences in the rate of mass transfer in the initial and final stages (rapid initial stage and slow second stage) of the sorption. This also implies that intra-particle diffusion was not the only rate controlling step but other surface phenomena were actively involved in the sorption process [41].

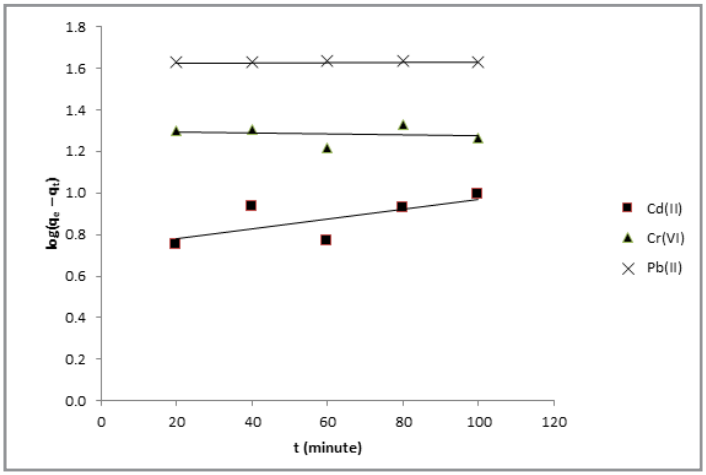

Figure 9: Variation of Log (Q_e – Q_t) With T for the Adsorption of Cd (II), Cr (VI) And Pb (II) Onto PU – IONP

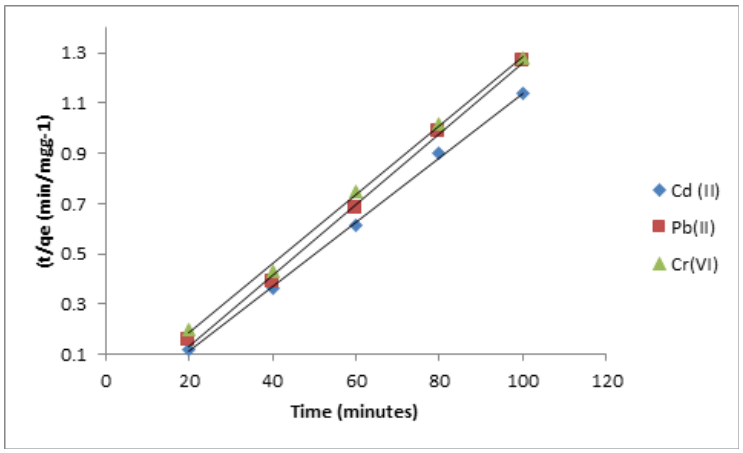

Figure 10: Variation of $\frac{t}{q_e}$ with t for the adsorption of Cd (II), Cr (VI) and Pb (II) onto PU – IONP

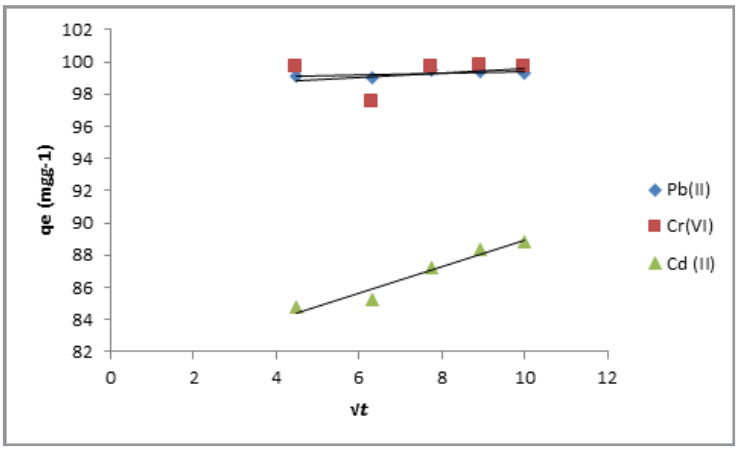

Figure 11: Variation of q_t with√t for the Adsorption of Cd (II), Cr (VI) and Pb (II) onto PU – IONP

Table 5: Intraparticle Diffusion, Pseudo First and Second Order Rate Constants for The Adsorption of Some Metal Ions by Pu - Ionp

Cation	Pseudo – first order			Pseudo – second order			intraparticle diffusion		
	qe (mg/g)	k1 (min^{-1})	R^2	qe (mg/g)	K^2 ($gmg^{-1}min^{-1}$)	R^2	β (mg/g)	k_{in}	R^2
Cd (II)	0.7302	0.0055272	0.4876	72.464	0.0014763	0.9991	80.77	0.8136	0.9478
Cr (VI)	1.2965	0.004606	0.0306	77.519	0.012059	0.9994	98.126	0.1494	0.1076
Pb (II)	1.6303	0.0000230	0.6327	70.922	0.0141	0.9993	98.853	0.0555	0.4309

Adsorption Isotherms

Three different isotherm models namely Dubinin – Radushkevich isotherm (D-R) model, Freundlich and Langmuir, were used to treat the generated equilibrium data from the batch experiments with the intention of proposing the adsorption process mechanism.

Langmuir Adsorption Isotherm

The linear form of the Langmuir adsorption isotherms is represented in equation 7 [42].

$$\frac{C_e}{q_e} = \frac{1}{bQ_m} - \frac{C_e}{Q_m} \quad (7)$$

where qe is the adsorbent metal ion quantity per gram of adsorbent at equilibrium (mgg^{-1}), Q_m is the maximum amount of metal ion per unit weight of adsorbent required to form a complete monolayer on the surface bound (mgg^{-1}), *b is* a constant which is related to the affinity of the binding sites (lmg^{-1}), C_e is the equilibrium concentration. Q_m and b can be respectively calculated from the slope and intercept of the straight lines plot of $\frac{C_e}{q_e}$ versus Ce.

The plots $\frac{C_e}{q_e}$ against Ce for Cd (II), Cr (VI) and Pb (II) adsorption onto PU – IONP are shown in Figures 12. The isotherm parameters (R^2, Q_m, R_L and b) derived from the slope and intercept of the Langmuir plot is as presented in Table 6. The values of maximum sorption capacity (Q_m) which correspond to the complete monolayer coverage for Cd (II), Cr (VI) and Pb (II) adsorption were found to be 322.5807 mg/g, -303.3333 mg/g and 322.5806 mg/g respectively. The small and negative Q_m values obtained for Cr (VI) signifies that its adsorption onto PU – IONP surface did not follow the Langmuir model and cannot be said to be a monolayer adsorption process. The separation factor or equilibrium parameter (R_L) for the adsorption process was evaluated using equation 8 [43].

$$R_L = \frac{1}{1 + bC_o} \quad (8)$$

where Co is the initial metal ion concentration (mgL^{-1}). The result obtained is as given in Table 6. It can be deduced from the result presented that the equilibrium parameter for Cd (II), Cr (VI) and Pb (II) are less than unity signifying that PU – IONP is an ideal adsorbent capable of adsorbing all the three metal ions selected in this study from aqueous medium. According to Soldatkina and Yanar [44], smaller R_L values imply more favourable relationship between the adsorbent and the adsorbate and hence higher adsorption. Since the R_L value obtained in the research followed this order: Cd (II) > Pb (II) > Cr (VI), it implies that in the aqueous solution, Cr (VI) will compete for the binding sites better and faster than Cd(II) and Pb (II) and further explains why the percentage adsorption of Cr (VI) was found to be higher than that of Cd (II) and Pb (II) in the study.

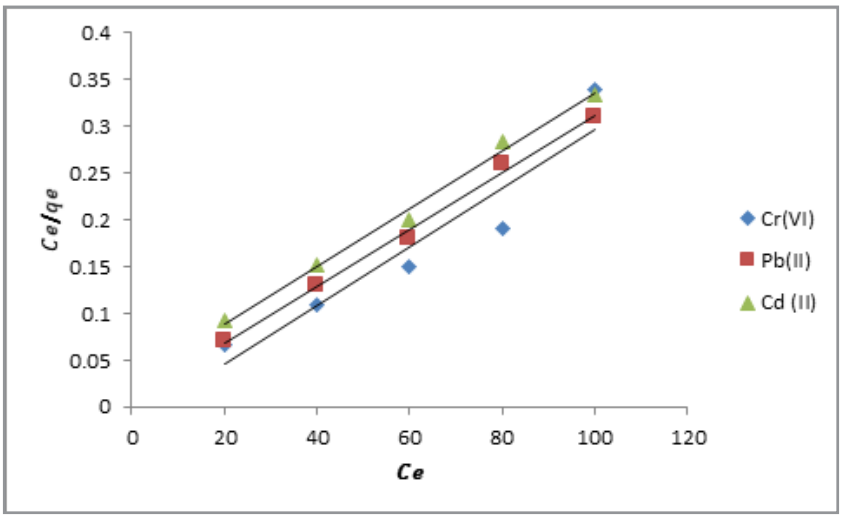

Figure 12: Langmuir Isotherm for The Adsorption of Cr (VI), Cd (II) And Pb (II) Ions by PU – IONP

Freundlich Isotherm

The equation for the Freundlich adsorption model can be written in the form given by equation 9 [45].

$$log(q_e) = logk_f + \frac{1}{n} logC_e \quad (9)$$

where k_f and n which are respectively the Freundlich's constants related to the adsorption capacity and adsorption intensity of the adsorbent.

Figure 13 shows the Fruendlich isotherm (linear plot of log q_e versus log C_e) obtained for the adsorption of Cr (VI), Cd (II) and Pb (II) ions from aqueous solution by PU – IONP. The Freundlich adsorption constants evaluated from the isotherms for Pb (II), Cd (II), and Cr (VI) ions are presented in Table 6. It can be seen from the results reported that the regression coefficient (R2) obtained for Cr (VI) adsorption in the Freundlich plot is unity (1.0). This value is slightly lower than the 0.9205 obtained for the same metal ion in Langmuir isotherm, an indication that the Freundlich model provides better fit for Cr (VI) adsorption in this study

The lower R^2 values obtained for Pb (II) and Cd (II) in Freundlich isotherm when compared with their values from the Langmuir model indicates that the Langmuir model is better fitted for Pb (II) and Cd (II) adsorption than the Freundlich model. This implies that the adsorption of Cr (VI) from the aqueous solution may have followed the heterogeneous route while that of Pb (II) and Cd (II) is more of a monolayer process.

The Freundlich parameter ($\frac{1}{n}$) have used to measure the adsorption intensity of adsorbates onto adsorbent surface in literature. Adsorption is considered favourable when n>1 (which means $\frac{1}{n}<1$) and unfavourable "n" values drop below 1 (or $\frac{1}{n}<1$). According to Edet and Ifelebuegu, the higher the value of "n", the stronger the interaction between the adsorbate and the adsorbent surface indicating a more intense and highly non – linear adsorption process. The higher "n" value obtained for Cr (VI) as noticed in Table 4.6 when compared with those of Pb (II) and Cd (II), indicates the preferential sorption of Cr (VI) than Cd (II) and Pb (II) onto PUF –IONP. These collaborated with our findings previously in this study.

The k_f value which is an indicator of the ability of PUF –IONP to remove the studied heavy metal ions from the aqueous medium even at high concentrations was estimated from the intercept of the Freundlich plots and reported in Table 6. Higher k_f values have been reported to signify higher maximum adsorption capacity. The k_f value of Cr (VI) (44.99 l/g) obtained is greater than that of Pb (II) (34.71 l/g) and Cd (II) (34.83 l/g). This suggests and confirms that Cr (VI) has greater tendency and ease of adsorption by PUF –IONP than the other two studied metal ions. This remarkable difference in the uptake of the studied metal ions by the adsorbent may be due to the considerable difference in their hydration radii and hydration enthalpies. The hydration radii of Cd (II), Pb (II) and Cr (VI) ions have been reported to be the 4.26 A°, 4.01A° and 1.96 A° respectively [46]. Ideally, the smaller cations are supposed to be adsorbed faster and in larger quantities than larger cations. This is because, the smaller the cations, the easier it will be to pass through the pores and channels of the adsorbent. Hence, the ions with smaller hydrated radius will have higher affinity to be adsorbed onto the PUF – IONP surface. This supports the order of sorption (Cr (VI) > Pb (II) > Cd (II)) for the studied metal ions by PUF – IONP obtained in this research.

The Fruendlich adsorption constant (K_F) is related to the free energy of adsorption according to equation 10.

$$\Delta G^0_{ads} = -2.303RTlogK_F \quad (10)$$

where R is the universal gas constant and T is the temperature. Values of ΔG^0_{ads} calculated from equation 10 are also presented in Table 6. From the table presented, it can be deduced that the free energies are negatively less than the threshold value of needed for the mechanism of chemisorption. Therefore, the adsorption of Cr (VI), Pb (II) and Cd (II) onto PU – IONP is spontaneous and is consistent with the mechanism of physical adsorption

Table 6: Freundlich and Langmuir Parameters for the Adsorption of Cr(VI), Pb(II) and Cd(II) by PU - IONP

Metal ion	Langmuir parameters				Freundlich parameters			
	Q_m (mgg^{-1})	b (lmg^{-1}),	R_L	R²	n	k_f	R²	ΔG⁰ (kJ/mol)
Cr (VI)	-303.3333	0.442857	0.022581	0.7027	1.30002	44.99	1.00	-9.590
Pb (II)	322.5806	0.182927	0.054667	0.9949	1.14929	34.71	0.9880	-8.937
Cd (II)	322.5806	0.111511	0.089677	0.994	1.14889	34.83	0.9912	-8.945

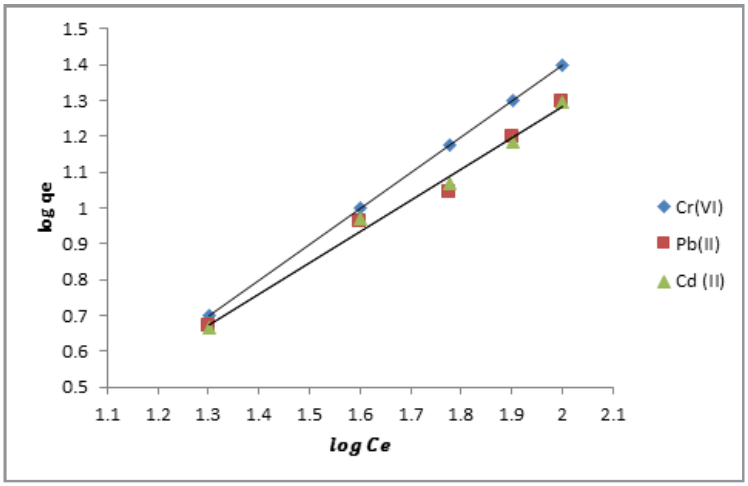

Figure 13: Fruendlich isotherm for the adsorption of Cr (VI), Cd (II) and Pb (II) ions from aqueous solution by PU – IONP

Dubinin–Radushkevich Isotherm (D-R) Model

The Dubinin–Radushkevich isotherm (D-R) model was used to evaluate the apparent energy of adsorption. The adsorption data were fitted into the Dubinin-Radushkevich (D-R) adsorption equation which is expressed as equation 11.

$$lnq_e = lnX_m - \beta\left(RTln\left(1+\frac{1}{C_e}\right)\right)^2 \quad (11)$$

where qe (mgl/g) is the concentration of the adsorbate adsorbed in the adsorbent, Xm (mg/g) is the maximum sorption capacity, R (kJ/mol/K) is the gas constant and T (K) is the temperature. β (mg²/kJ²) is a constant related to the mean adsorption energy (E) which can be estimated from equation 12.

$$E = \frac{1}{(2\beta)^{\frac{1}{2}}} \quad (12)$$

From equation 12, a plot of lnq_e versus $(RTln\left(1+\frac{1}{C_e}\right))^2$ should give a straight line with slope and intercept equal to β and lnX_m respectively. The Dubinin-Radushkevich isotherms derived for the adsorption of Pb (II), Cr (VI) and Cd (II) ions by PU – IONP is presented in Figure 14 while adsorption parameters deduced from the plots are given in Table 7. A closer look at the regression coefficient (R²) values obtained indicated that the D –R model also provides a good fit for the adsorption of the studied metals ions from aqueous solution since the R² values obtained were almost unity. The mean adsorption energy (E) for the adsorption process estimated from equation 8 for the three studied metals ions were found to be in the range of 1.186 - 1.266 kJ/mol. These values are less than the threshold value of 8 kJ/mol required for chemical adsorption [36]. This further supports our accession that the adsorption of Pb (II), Cr (VI) and Cd (II) ions by PU – IONP is consistent with the mechanism of physical adsorption.

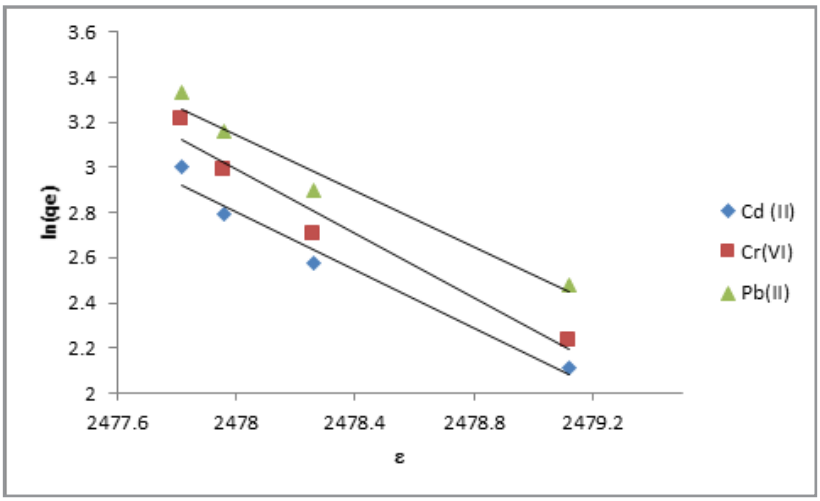

Figure 14: Variation of log(q_e) with ε for the adsorption of Cr (VI), Cd (II) and Pb (II) ions from aqueous solution by PU – IONP

Table 7: D-R Parameters for the Adsorption of Cr (VI), Cd (II) and Pb (II) ions from Aqueous Solution by PU – IONP

Metal ion	β(mg²/kJ²)	ln (X_m)	E (kJ/mol)	R²
Cr (VI)	0.7111	1765.1	1.186	0.9587
Pb (II)	0.6242	1549.9	1.266	0.9674
Cd (II)	0.6454	1602.2	1.245	0.9729

Regeneration and Reusability of PU – IONP

According to Zhang et al (2019), the stability and regeneration ability of used adsorbent during adsorption process are essential to its practical application. The reusability studies were carried out to evaluate the number of times PU – IONP can be utilized for the removal of Pb (II), Cr (VI) and Cd (II) ions from aqueous solution while maintaining maximum extraction recovery. Figure 15 shows the percentage recovery (% R) achieved for each of the studied metal ion after fifteen successive adsorption–desorption cycles. A closer examination of the plots reveals that the extraction capacity of PU – IONP remains unchanged even after six regeneration cycles for Pb (II) ion, eight cycles for Cr (VI) and five cycles for Cd (II) ion. The extraction recovery gradually decreased by a small margin after seven cycles for Pb (II), nine cycles for Cr (VI) and six cycles for Cd (II). Based on these observations, we can say that PU – IONP can be regenerated and reused in practical wastewater treatment due to its excellent adsorption performance and regeneration.

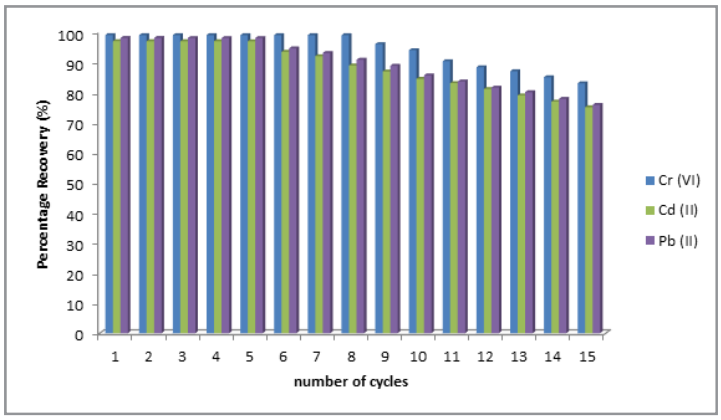

Figure 15: Reusability (Recovery Number of Cycles) of PU – IONP

Cost of The Adsorption Operation

The economic viability of PU – IONP was accessed by comparing the cost of the adsorbent per gram of adsorbate removed with that of other well-known adsorbents. The cost of the adsorption operation was estimated by determining the cost of the prepared adsorbent per gram of adsorbate as shown in equation 13 [47].

Adsorption cost USD/g adsorbate = [Chemical Purchase cost

$$\text{Adsorption cost}\ \frac{USD}{g_{adsorbate}} = \frac{\left[\text{Chemical Purchase cost}\left(\frac{USD}{g}\right) + \text{Energy Cost}\left(\frac{USD}{g}\right) kwh\right]}{\text{Adsorption capacity}\left(\frac{mg}{g}\right) \times 10^{-3}\left(\frac{g}{mg}\right)} \quad (13)$$

Where the adsorption capacity is the amount of adsorbate removed per adsorbent used in mg/g. In this study, we found that the cost of producing PUF – IONP is estimated to be 0.19 $/kg, which is significantly lower than the market price of activated carbon and other adsorbents. The use of PUF – IONP for instance in the removal of 1 g of Pb (II) ions from solution was found to be cheaper (0.1411 $) than the nano-zeolite and Coconut shell biochar (0.7183 and 0.6945 $), respectively. Table 8 further compares our findings to the results of other experiments conducted under various circumstances for several adsorbents [48-50]. From the Table, it is evident that the newly synthesized PUF - IONP is very suitable in the treatment of waste water. According to Ighalo et al [47], adsorbents at 1 $/mol threshold can be considered very cheap for the intended application, while those at 200 $/mol can be considered very expensive. Since the cost of our prepared adsorbent falls below the 1 $/mol threshold (which may have arisen from the low cost and availability of some of the raw materials and the overall cost of consumption of electricity used in the synthesis of PIN process), it can be regarded as a cheap adsorbent [51-53].

Table 8: Comparison of Performances of PUF – IONP with Different Adsorbent in Literature

S/N	Adsorbent name	Target Contaminant	Adsorption capacity (mg/g)	Cost ($/g)	Reference
1	Cation-exchange resin	Ni (II)	63 0	000006	[48]
2	PVA/PEI electrospun nanofibers	Phosphorus	165.9	0.6495	[49]
3	Chitosan/cellulose	Cr(VI)	217.8	0.6200	[50]
4	Cherry kernels biochar	Pb (II)	94.48	0.419	[51]
5	Cherry kernels biochar	Cd (II)	92.42	0.419	[51]
6	Hierarchical ZnS-Ga2S3 G	Cr(VI)	54.42	0.0895	[52]
7	Chitosan-calcite	Pb (II)	21.36	0.2646	[53]
8	PUF -IONP	Pb (II)	228.4	0.1411	This experiment
9	PUF -IONP	Cd (II)	238.6	0.1411	This experiment

Conclusion

At the end of the study, the following conclusion can be drawn

- PUF – IONP composite synthesized by loading iron oxide nanoparticles inside a polyurethane (PU) foam matrix demonstrated excellent capacity to remove contaminants from River wudil
- The turbidity, chemical oxygen demand, biochemical oxygen demand, lead, nickel, cadmium values of the River water were reduced by 98.89 %, 86.51 %, 59.44 %, 90.00 %, 83.33 % and 80.00 % respectively when the it was treated with the adsorbent
- The adsorption of the pollutants onto PUF - IONP was spontaneous, feasible, followed a second order kinetic model and is consistent with the mechanism of physical adsorption
- The cost of the prepared adsorbent falls below the 1 $ / mol threshold and hence can be regarded as a cheap adsorbent
- PU – IONP can be regenerated and reused in practical wastewater treatment due to its excellent adsorption performance and regeneration
- The result of this study creates a base for the use of PUF – IONP large-scale production of non-conventional adsorbents, thereby offering a lot of promising benefits for commercial purposes in the future

Acknowledgments

The author is grateful to the Tertiary Education Trust Fund of Nigeria (TETFUND) for the funding he received in executing this research

Competing Interests

The authors declare no competing interests.

Data Availability Statement

The datasets used or analyzed during the current study are available from the corresponding author upon reasonable request.

References

1. Suleiman, A. U., Dogarai, S. B. B., Kwazo, H. A., Mohammed, S., & Bagna, E. (2020). Extraction of heavy metal in tannery effluent using abundant agricultural wastes. International Journal of Science for Global Sustainability, 6, 48–55. https://fugus-ijsgs.com.ng/index.php/ijsgs/article/view/6
2. Ighalo, J. O., & Adeniyi, A. G. (2020). A comprehensive review of water quality monitoring and assessment in Nigeria. Chemosphere, 260, 127569. https://doi.org/10.1016/j.chemosphere.2020.127569
3. Shawai, S. A. A., Abubakar, B. B., Nahannu, M. S., & Gaya, H. S. (2019). Status of water used for drinking and irrigation in Kano: A critical review on physicochemical and heavy metals concentration. American Journal of Biomedical Science & Research, 5, 235–242. https://doi.org/10.34297/AJBSR.2019.05.000918
4. Ameh, P. O. (2022). Utilization of nanoparticle prepared from local Nigerian hen egg shell as an adsorbent for the removal of methylene blue dye from aqueous solution: DFT and experimental study. Chemical Review Letters, 5, 29–43. https://doi.org/10.22034/crl.2023.328721.1155
5. Eddy, N. O., Ukpe, R. A., Garg, R., Garg, R., Odionenyi, A. O., Ameh, P., & Akpet, I. (2024). Enhancing water purification efficiency through adsorption and photocatalysis: Models, application and challenges. International Journal of Environmental Analytical Chemistry. https://doi.org/10.1080/03067319.2023.2295934
6. Ahmed, S. F., Mofijur, M., Parisa, T. A., Islam, N., Kusumo, F., Inayat, A., Le, V. G., Badruddin, I. A., Khan, T. M. Y., & Ong, H. C. (2022). Progress and challenges of contaminant removal from wastewater using microalgae biomass. Chemosphere, 286(Pt. 1), 131656. https://doi.org/10.1016/j.chemosphere.2021.131656
7. Habu, M. A., Bawa, U., & Musa, S. I. (2021). Health risk assessment and heavy metal bioaccumulation in vegetables irrigated with wastewater in Kano State, Nigeria. Notulae Scientia Biologicae, 13, 1–8. https://doi.org/10.15835/nsb13110890
8. Aziz, K. H. H., Mustafa, E., Omer, K. M., Hama, S., Hamarwi, R. F., & Rahman, K. O. (2023). Heavy metal pollution in the aquatic environment: Efficient and low-cost removal approaches to eliminate their toxicity: A review. RSC Advances, 13(26), 17595–17610. https://doi.org/10.1039/D3RA00723E
9. Narayana, P. L., Maurya, A. K., Wang, X., Harsha, M. R., Srikanth, O., Alnuaim, A. A., Hatamleh, W. A., Hatamleh, A. A., Cho, K. K., Paturi, U. M. R., & Reddy, B. S. (2021). Artificial neural networks modeling for lead removal from aqueous solutions using iron oxide nanocomposites from bio-waste mass. Environmental Research, 199, 111370. https://doi.org/10.1016/j.envres.2021.111370
10. Qasem, N. A. A., Mohammed, R. H., & Lawal, D. U. (2021). Removal of heavy metal ions from wastewater: A comprehensive and critical review. npj Clean Water, 4, 36. https://doi.org/10.1038/s41545-021-00127-0
11. Eddy, P. O., Ameh, P. O., Edet, U. E., Oladele, J. O., Kelle, H. I., Ogoko, E. C., Odiongenyi, A. O., Ukpe, R. A., Ogbodo, R., Garg, R., & Rishav, G. (2023). Synthesis and application of novel microporous framework of nanocomposite from trona for photocatalysed degradation of methyl orange dye. Environmental Monitoring and Assessment, 195, 1416. https://doi.org/10.1007/s10661-023-12014-x
12. Maftouh, A., El Fatni, O., El Hajjaji, S., Jawish, M. W., & Sillanpää, M. (2023). Comparative review of different adsorption techniques used in heavy metals removal in water. Biointerface Research in Applied Chemistry, 13(4), 397. https://doi.org/10.33263/BRIAC134.397
13. Chowdhury, I. R., Chowdhury, S., Mazumder, M. A. J., & Al-Ahmed, A. (2022). Removal of lead ions (Pb^{2+}) from water and wastewater: A review on the low-cost adsorbents. Applied Water Science, 12(8), 185. https://doi.org/10.1007/s13201-022-01703-6
14. Motitswe, M. G., Badmus, K. O., & Khotseng, L. (2022). Development of adsorptive materials for selective removal of toxic metals in wastewater: A review. Catalysts, 12(9), 1057. https://doi.org/10.3390/catal12091057
15. Essien, U. I., Odiongenyi, A. O., Obadimu, C. O., & Obdimu, I. S. (2023). Investigation of snail shells as an adsorbent and precursor for the synthesis of calcium oxide nanoparticles for the removal of amoxicillin from aqueous solution. Communication in Physical Sciences, 8(4), 453–464. https://journalcps.com/index.php/volumes/article/view/158
16. Gunashekar, S., & Abu-Zahra, N. (2014). Characterization of functionalized polyurethane foam for lead ion removal from water. International Journal of Polymer Science, 1–7.

https://doi.org/10.1155/2014/570309
17. Teodosiu, C., Wenkert, R., Tofan, L., & Paduraru, C. (2014). Advances in preconcentration/removal of environmentally relevant heavy metal ions from water and wastewater by sorbents based on polyurethane foam. Reviews in Chemical Engineering, 30(4), 403–420. https://doi.org/10.1515/revce-2013-0035
18. Zhang, Z., Zhu, L., & Jin, J. (2017). Preparation of polyurethane foam adsorbents and their application on preconcentration/removal of metal ions. Materials Review, 31, 34–39. https://doi.org/10.11896/j.issn.1005-023X.2017.05.006
19. Iqhrammullah, M., Hedwig, M. R., Karnadi, I., Kurniawan, K. H., Olaiya, N. G., & Abdulmadjid, S. N. (2020). Filler-modified castor oil-based polyurethane foam for the removal of aqueous heavy metals detected using laser-induced breakdown spectroscopy (LIBS) technique. Polymers, 12(4), 903. https://doi.org/10.3390/polym12040903
20. Koronis, G., Silva, A., & Fontul, M. (2013). Green composites: A review of adequate materials for automotive applications. Composites Part B: Engineering, 44(1), 120–127. https://doi.org/10.1016/j.compositesb.2012.07.004
21. Stavrinou, A., Aggelopoulos, C. A., & Tsakiroglou, C. D. (2018). Exploring the adsorption mechanisms of cationic and anionic dyes onto agricultural waste peels of banana, cucumber and potato: Adsorption kinetics and equilibrium isotherms as a tool. Journal of Environmental Chemical Engineering, 6, 6958–6970. https://doi.org/10.1016/j.jece.2018.10.063
22. Sani, A., Musa, M. U., Adamu, U. K., Sanda, A. R., Adam, I. A., & Almu, H. (2020). River water quality assessment and suitability for irrigation in Northern Sudan Savanna ecological zone of Nigeria. International Journal of Environment and Pollution Research, 8(3), 30–40.
23. American Public Health Association. (2022). Standard methods for the examination of water and wastewater (24th ed.; A. D. Eaton, L. S. Clescer, E. W. Rice, & A. E. Greenberg, Eds.). Port City Press.
24. Ameh, P. O. (2023). Synthesized iron oxide nanoparticles from Acacia nilotica leaves for the sequestration of some heavy metal ions in aqueous solutions. Journal of Chemistry Letters, 4(1), 1–13. https://doi.org/10.22034/jchemlett.2023.360137.1083
25. Dinali, R., Ebrahiminezhad, A., Manley-Harris, Y., Ghasemi, Y., & Berenjian, A. (2017). Iron oxide nanoparticles in modern microbiology and biotechnology. Critical Reviews in Microbiology, 43, 493–507. https://doi.org/10.1080/1040841X.2016.1267708
26. Gunashekar, S. (2015). A study on the synthesis-structure-performance relationship of bulk functionalized polyurethane foams for water filtration applications [Doctoral dissertation, University of Wisconsin-Milwaukee].
27. Kongsat, P., Kudkaew, K., Tangjai, J., O'Rear, E. A., & Pongprayoon, T. (2021). Synthesis of structure controlled hematite nanoparticles by a surfactant-assisted hydrothermal method and property analysis. Journal of Physics and Chemistry of Solids, 148, 109685. https://doi.org/10.1016/j.jpcs.2020.109681
28. Jamila, T. S., & Sule, S. Y. (2020). Assessments of quality index of river Getsi irrigation water in Kano Metropolis, Nigeria. International Research Journal of Pure and Applied Chemistry, 21, 8–16. https://doi.org/10.9734/irjpac/2020/v21i330156
29. Agbazue, V. E., Ekere, N. R., & Samira, M. I. (2015). Physico-chemical parameters and heavy metal levels in water and fish samples from River Jakara and Jakara Dam, Kano State, Nigeria. Asian Journal of Chemistry, 27, 3794–3798. https://doi.org/10.14233/ajchem.2015.18993
30. National Environmental Standards and Regulations Enforcement Agency. (2021). Federal water quality standard. NESREA Act 25, 5–21.
31. World Health Organization. (2022). Guidelines for drinking-water quality: Fourth edition incorporating the first and second addendum. World Health Organization.
32. Ekevwe, A. E., Isaac, A., Bartholomew, G., & Aroh, A. O. (2018). Review of organic pollutants in wastewater along the course of River Gwagwarwa and River Rafin Malam in Kano State, Nigeria. Journal of Biotechnology and Bioengineering, 2, 36–39. https://doi.org/10.22259/2637-5362.0202006
33. Ibrahim, S., & Sa'id, H. (2010). Heavy metals load in tilapia species: A case study of Jakara River and Kusalla Dam, Kano State, Nigeria. BAJOPAS, 3, 87–90. https://doi.org/10.4314/bajopas.v3i1.58721
34. Okon, I. E., Anweting, I. B., & Nwokem, N. A. (2022). A study on heavy metals pollution levels in water and sediment of River Kubani Dam, Zaria, Nigeria. Pacific Journal of Science and Technology, 23(2), 107–116.
35. Ogoko, E. C., Kelle, H. I., Akintola, O., & Eddy, N. O. (2023). Experimental and theoretical investigation of Crassostrea gigas shell-based CaO nanoparticles as a photocatalyst for the degradation of bromocresol green dye (BCGD) in an aqueous solution. Biomass Conversion and Biorefinery. https://doi.org/10.1007/s13399-023-03742-8
36. Odoemelam, S. A., Emeh, N. U., & Eddy, N. O. (2018). Experimental and computational chemistry studies on the removal of methylene blue and malachite green dyes from aqueous solution by neem (Azadirachta indica) leaves. Journal of Taibah University for Science, 12(3), 255–265. https://doi.org/10.1080/16583655.2018.1465725
37. Tejada-Tovar, C., Villabona-Ortíz, A., & González-Delgado, Á. D. (2023). High-efficiency removal of lead and nickel using four inert dry biomasses: Insights into the adsorption mechanisms. Materials, 16, 4884. https://doi.org/10.3390/ma16134884
38. Revellame, E. D., Fortela, D. L., Sharp, W., Hernandez, R., & Zappi, M. E. (2020). Adsorption kinetic modeling using pseudo-first order and pseudo-second order rate laws: A review. Cleaner Engineering and Technology, 1, 100032. https://doi.org/10.1016/j.clet.2020.100032
39. Kostoglou, M., & Karapantsios, T. D. (2022). Why is the linearized form of pseudo-second order adsorption kinetic model so successful in fitting batch adsorption experimental data? Colloids and Interfaces, 6, 55. https://doi.org/10.3390/colloids6040055
40. Wang, J., & Guo, X. (2022). Rethinking of the intraparticle diffusion adsorption kinetics model: Interpretation, solving methods and applications. Chemosphere, 309(2), 136732. https://doi.org/10.1016/j.chemosphere.2022.136732
41. Vareda, J. P. (2023). On validity, physical meaning, mechanism insights and regression of adsorption kinetic models. Journal of Molecular Liquids, 376, 121416. https://doi.org/10.1016/j.molliq.2023.121416

42. Edet, U. A., & Ifelebuegu, A. O. (2020). Kinetics, isotherms, and thermodynamic modeling of the adsorption of phosphates from model wastewater using recycled brick waste. Processes, 8, 665. https://doi.org/10.3390/pr8060665
43. Hasani, N., Selimi, T., Mele, A., Thaçi, V., Halili, J., Berisha, A., & Sadiku, M. (2022). Theoretical, equilibrium, kinetics and thermodynamic investigations of methylene blue adsorption onto lignite coal. Molecules, 27, 1856. https://doi.org/10.3390/molecules27061856
44. Soldatkina, L., & Yanar, M. (2021). Equilibrium, kinetic, and thermodynamic studies of cationic dyes adsorption on corn stalks modified by citric acid. Colloids and Interfaces, 5(4), 52. https://doi.org/10.3390/colloids5040052
45. Ramos-Guivar, J. A., Checca-Huaman, N. R., Litterst, F. J., & Passamani, E. C. (2023). Surface adsorption mechanism between lead(II, IV) and nanomaghemite studied on polluted water samples collected from the Peruvian rivers Mantaro and Cumbaza. Nanomaterials, 13(10), 1684. https://doi.org/10.3390/nano13101684
46. Afrodita, Z., & Mirjana, G. (2014). Effect of competing cations (Cu, Zn, Mn, Pb) adsorbed by natural zeolite. International Journal of Science, Engineering and Technology, 2(5), 483–492.
47. Ighalo, J. O., Omoarukhe, F. O., Ojukwu, V. E., Iwuozor, K. O., & Igwegbe, C. A. (2022). Cost of adsorbent preparation and usage in wastewater treatment: A review. Cleaner Chemical Engineering, 3, 100042. https://doi.org/10.1016/j.clce.2022.100042
48. Li, T., Xiao, K., Yang, B., Peng, G., Liu, F., Tao, L., Chen, S., Wei, H., Yu, G., & Deng, S. (2019). Recovery of Ni(II) from real electroplating wastewater using fixed-bed resin adsorption and subsequent electrodeposition. Frontiers of Environmental Science & Engineering, 13(6), 1–12. https://doi.org/10.1007/s11783-019-1175-7
49. Li, S., Huang, X., Liu, J., Lu, L., Peng, K., Bhattarai, R., & [additional authors if applicable]. (2020). PVA/PEI crosslinked electrospun nanofibers with embedded $La(OH)_3$ nanorod for selective adsorption of high flux low concentration phosphorus. Journal of Hazardous Materials, 384, 121457. https://doi.org/10.1016/j.jhazmat.2019.121457
50. Zeng, H., Hu, Z., Peng, C., Deng, L., Liu, S., & [additional authors if applicable]. (2021). Effective adsorption and sensitive detection of Cr(VI) by chitosan/cellulose nanocrystals grafted with carbon dots composite hydrogel. Polymers, 13(21), 3788. https://doi.org/10.3390/polym13213788
51. Vukelić, D., Bošković, N., Agarski, B., Radonić, J., Budak, I., Pap, S., & Sekulić, M. T. (2018). Eco-design of a low-cost adsorbent produced from waste cherry kernels. Journal of Cleaner Production, 174, 1620–1628. https://doi.org/10.1016/j.jclepro.2017.11.098
52. Qi, Y., Fan, Y., Liu, T., & Zheng, X. (2020). Flower-like hierarchical ZnS-Ga_2S_3 heterojunction for the adsorption-photo-reduction of Cr(VI). Chemosphere, 261, 127824. https://doi.org/10.1016/j.chemosphere.2020.127824
53. Pap, S., Kirk, C., Bremner, B., Sekulić, M. T., Shearer, L., Gibb, S. W., & Taggart, M. A. (2020). Low-cost chitosan-calcite adsorbent development for potential phosphate removal and recovery from wastewater effluent. Water Research, 173, 115573. https://doi.org/10.1016/j.watres.2020.115573

Copyright: *©2026 Paul Ocheje Ameh. This is an open-access article distributed under the terms of the Creative Commons Attribution License, which permits unrestricted use, distribution, and reproduction in any medium, provided the original author and source are credited.*